Acta Mech 232, 1113–1129 (2021)
https://doi.org/10.1007/s00707-020-02812-6

ORIGINAL PAPER

Hui Qi · Fuqing Chu · Jing Guo · Ruochen Sun

Dynamic analysis for a vertical interface crack and the nearby circular cavity located at the piezoelectric bi-material half-space under SH-waves

Received: 16 July 2019 / Revised: 22 July 2020 / Accepted: 5 September 2020 / Published online: 9 January 2021

Abstract The present problem aims to study the scattering behavior of SH-waves by a circular cavity near two symmetrically permeable interface cracks in the piezoelectric bi-material half-space. The steady-state response of the problem is obtained, with the aid of the Green's function method and the complex function method. Above all, the essential expression of Green's function is constructed by the mirror method. This expression satisfies the conditions of being stress-free and electric insulation on the horizontal boundary of the orthogonal space where the circular cavity is located, and the condition of bearing a harmonic out-plane line source force on the vertical boundary. Next, on the basis of dividing the bi-material medium into two parts along the vertical boundary, the first kind of Fredholm integral equation with uncertain anti-plane forces is established by using the conjunction method and the crack-division technology. Then, the solution is obtained by solving an algebraic equation with finite terms, which is an effective truncation of the integral equation. Finally, the dynamic stress concentration factor around the edge of the circular cavity and the dynamic stress intensity factor at the crack tip are calculated numerically. On this basis, the effects of incident wave frequency, crack length, crack location and circular cavity position on the dynamic stress concentration factor and dynamic stress intensity factor are discussed.

1 Introduction

Piezoelectricity, also known as electromechanical coupling, is the property that certain materials acquire a charge when they are compressed, twisted, or deformed. Due to the electromechanical coupling effect, piezoelectric materials can not only realize the exchange of the mechanical vibration and alternating current but also realize self-diagnosis and self-repair of structures. This makes piezoelectric materials widely used in smart structures and sensor elements, and play a critical role in aviation detection, marine sonar, urban development, new energy research and development, national defense and the military industry. However, piezoelectric materials may cause equipment failure under electrical and mechanical loads due to brittleness and defects, affecting the normal use and reliability of the equipment. These defects may be caused by processing technologies, environmental changes and production processes, such as cavities in piezoelectric materials, interface cracks caused by the fracture of different materials, and so on. Or they are artificially added in order to improve the performance of the material, such as in porous piezoelectric materials. The dynamic stress concentration at the crack tip and around the cavity in piezoelectric materials is more complex than in ordinary materials. So, many studies [1–14] have focused on the scattering behavior of elastic waves by the defects in piezoelectric materials.

Previously, Shu [10] analyzed the solutions of orthogonally laminated piezoelectric composite plates under different boundary conditions by the equivalent single layer theory. Wang [12] investigated the anti-plane

H. Qi · F. Chu · J. Guo (✉) · R. Sun
College of Aerospace and Civil Engineering, Harbin Engineering University, Harbin 150001, Heilongjiang, China
E-mail: gj3041@126.com

problem of a crack near an elliptical cavity in isotropic piezoelectric bi-materials using Stroh's theory. Song and Shindo used the function expansion method to study the dynamic characteristics of the circular rigid inclusion [4], the circular hole [3], the impermeable crack [7], and the circular piezoelectric inclusion [2] in infinite piezoelectric materials, respectively. Du [1] applied the permeable crack model to investigate the scattering problems of an anti-plane shear wave caused by partial debonding around a circular inclusion. Feng [5] discussed the scattering of an SH-wave on the debonding inclusion in piezoelectric material via the singular integral equation technique. Yang [8] studied the interaction of N randomly distributed cylindrical inclusions in the piezoelectric matrix. In terms of piezoelectric bi-materials, Song et al. further studied the dynamic problems of an impermeable crack [11], a circular cavity near the interface [15], and a circular cavity with interface crack [9] in piezoelectric bi-materials.

The SH-wave scattering problem, as the simplest elastic wave scattering problem, has a relatively mature theory, but there are still many boundary value problems that have not been solved. Few papers have studied the problem of elastic wave scattering in a homogeneous isotropic piezoelectric bi-material half-space. Although many valuable results have been achieved, they all belong to the global space [9,11,15]. Based on our previous researches on the problem of SH-wave scattering in elastic bi-materials [16], we further extended this research to bi-material piezoelectric materials. In a previous article by Qi [13], an exact, analytical solution to the boundary-value problem of the two-dimensional scattering of anti-plane (SH) waves by a circular inclusion near the interface cracks in the piezoelectric bi-material half-space was presented. However, due to the existence of standing waves in the inclusion, the dynamic performance of the circular cavity and circular inclusion subject to the SH-waves is quite different [3,4]. Therefore, in order to enrich the scattering problems in the piezoelectric bi-material half-space, this paper studies the problem of SH-wave scattering by a circular cavity near the interface crack in the piezoelectric bi-material half-space. For this issue, the Green's function method and the complex function method are used, the boundary conditions of defects are assumed to be stress-free and electrically permeable, and besides, the analytic expression of the wave function is obtained by the mirror method. Finally, the dynamic stress concentration factors around the circular cavity and the dynamic stress intensity factor at the crack tip are given. Those results demonstrate that the influence of interface crack can not be ignored.

2 Theoretical model

Figure 1 provides a half-space model of the piezoelectric bi-material with a vertical interface crack and a circular cavity nearby. As the figure shows, the isotropic plane which is subjected to out-of-plane displacement and in-plane electric field lies in the xy plane, while the polarization direction of the isotropic plane is along the z-axis. There are two mediums in the figure. Medium I is the right-angle space with a circular cavity and a permeable crack, while medium II is the right-angle space with a permeable crack. In medium I, Γ_{H}: horizontal boundary; Γ_{V}:vertical boundary; a: radius of cavity; ρ_1: mass density; c_{44}^{I}: shearing modulus; e_{15}^{I}: piezoelectric constant; κ_{11}^{I}: dielectric constant; e_{15}^{c} and κ_{11}^{c}: piezoelectric constant and dielectric constant of the cavity, respectively; h and d: the distance from the center of the circular cavity to the horizontal and vertical boundary, respectively. In medium II, ρ_1: mass density; c_{44}^{I}: shearing modulus; e_{15}^{I}: piezoelectric constant; κ_{11}^{I}: dielectric constant; A: half-length of the vertical interface crack; h_1: distance from the crack tip to the horizontal boundary.

The local coordinate system $x'o'y'$ is established at the center of the crack. The complex coordinate systems corresponding to the global coordinate system xoy and the local coordinate system $x'o'y'$ are $\eta = x+yi = re^{i\theta}$ and $\eta' = x' + y'i = r'e^{i\theta'}$, respectively. The relationships between the local and the global are:

$$\begin{cases} x' = x - d, \\ y' = y + h_1 + A - h. \end{cases} \tag{1}$$

Let an SH-wave propagate from medium I to medium II at an incident angle α_0 relative to the positive x-axis. When the SH-wave is applied on the medium I, the scattering wave can be produced and propagate away from the center of the circular cavity. Then, the scattering wave is reflected and refracted at the vertical interface, but the expressions of the reflected wave and refracted wave are complicated. In order to overcome this barrier, the bi-material half-space is divided into two right-angle spaces in Sect. 4. First, the left right-angle space with the circular cavity is investigated. By means of the mirror method, the expression of the scattering wave is obtained, which satisfies the stress-free and electric insulation conditions on the line boundaries. Second,

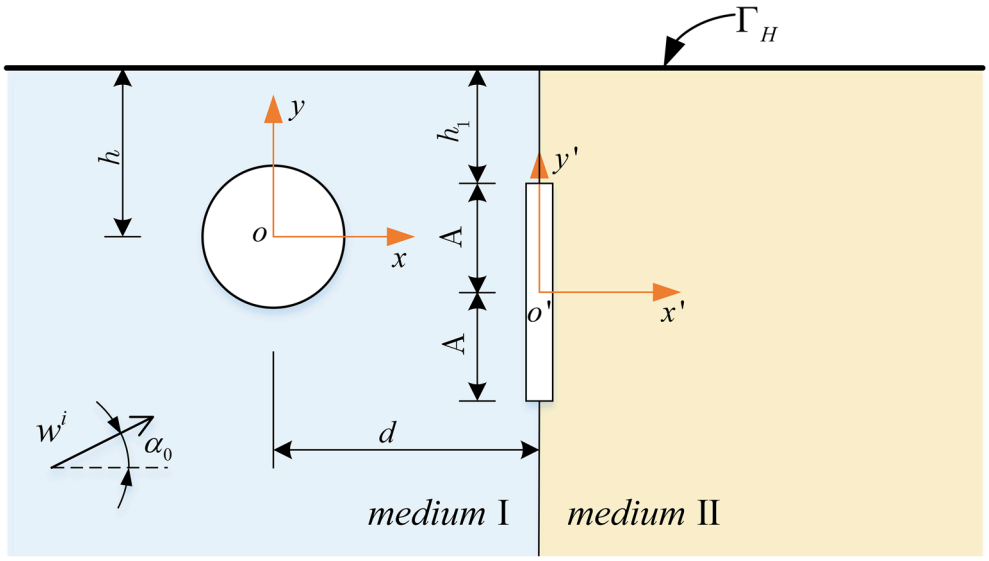

Fig. 1 The model of a piezoelectric bi-material half -space with a circular cavity and interface cracks

with the aid of the conjunction method, unknown anti-plane forces are applied on the vertical boundaries to satisfy the continuity condition on the vertical boundary of the two right-angle spaces. So, the two right-angle spaces could be thought of as a whole half-space. However, it is difficult to solve for the unknown anti-plane forces in Sect. 4. The Green's function method is applied, because anti-plane forces consist of a large number of line source forces. Thus, the expression of the Green's function related to the right-angle space containing the circular cavity and bearing the line source force is obtained in Sect. 3, which is the foundation to solve for the unknown anti-plane forces in Sect. 4.

The engineering background of the model in this paper is common in practical projects. For example, cavities and fractures in piezoelectric elements or piezoelectric plates could be caused by processing technologies, environmental changes, and production processes. These examples could be simplified as the model in this study when they are subjected to plane waves.

3 Green's function

The polarization direction is along the z-axis, and the time harmonic factor $e^{-i\omega t}$ is omitted. Taking the absence of body forces and free charges into account, the steady-state equilibrium equations are expressed as follows:

$$\begin{aligned} c_{44}\nabla^2 w + e_{15}\nabla^2\phi + \rho\omega^2 w = 0, \\ e_{15}\nabla^2 w - \kappa_{11}\nabla^2\phi = 0, \end{aligned} \tag{2}$$

where w, ϕ and ω stand for anti-plane displacement, electric potential and circular frequency, respectively. Equation (2) can be simplified as follows:

$$\nabla^2 w + k^2 w = 0, \quad \phi = \frac{e_{15}}{\kappa_{11}}(w + f), \quad \nabla^2 f = 0 \tag{3}$$

where the wavenumber $k = \rho\omega^2/c^*$, and the effective piezoelectric stiffness $c^* = c_{44} + e_{15}^2/\kappa_{11}$. These equations describe the electro-mechanical behavior of a homogeneous and isotropic piezoelectric material under anti-plane mechanical and in-plane electrical loading.

By means of the complex function method, complex variables $\eta = x + yi$, $\bar{\eta} = x - yi$ are introduced. In complex coordinates, Eq. (3) can be expressed as follows:

$$\frac{\partial^2 w}{\partial\eta\partial\bar{\eta}} + \frac{1}{4}k^2 w = 0, \quad \phi = \frac{e_{15}}{\kappa_{11}}(w + f), \quad \frac{\partial^2 f}{\partial\eta\partial\bar{\eta}} = 0. \tag{4}$$

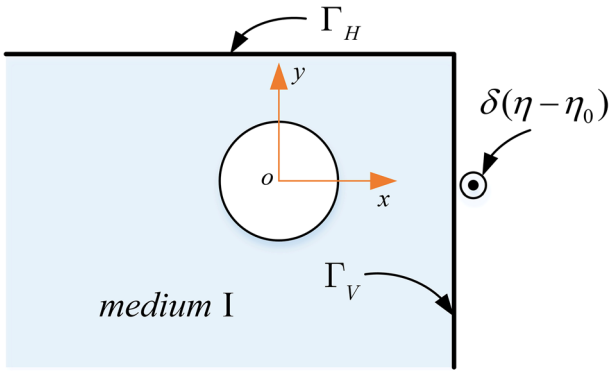

Fig. 2 The right-angle plane model impacted by a line source force

Introducing complex variables $\eta = re^{i\theta}$, $\bar{\eta} = re^{-i\theta}$, the anti-plane shear stress components (τ_{rz} and $\tau_{\theta z}$) and the in-plane electric displacement components (D_r and D_θ) can be expressed as:

$$\begin{aligned}
\tau_{rz} &= \left(c_{44} + \frac{e_{15}^2}{\kappa_{11}}\right)\left(\frac{\partial w}{\partial \eta}e^{i\theta} + \frac{\partial w}{\partial \bar{\eta}}e^{-i\theta}\right) + \frac{e_{15}^2}{\kappa_{11}}\left(\frac{\partial f}{\partial \eta}e^{i\theta} + \frac{\partial f}{\partial \bar{\eta}}e^{-i\theta}\right),\\
\tau_{\theta z} &= \left(c_{44} + \frac{e_{15}^2}{\kappa_{11}}\right) i\left(\frac{\partial w}{\partial \eta}e^{i\theta} - \frac{\partial w}{\partial \bar{\eta}}e^{-i\theta}\right) + \frac{e_{15}^2}{\kappa_{11}} i\left(\frac{\partial f}{\partial \eta}e^{i\theta} - \frac{\partial f}{\partial \bar{\eta}}e^{-i\theta}\right),\\
D_r &= -e_{15}\left(\frac{\partial f}{\partial \eta}e^{i\theta} + \frac{\partial f}{\partial \bar{\eta}}e^{-i\theta}\right),\\
D_\theta &= -e_{15} i\left(\frac{\partial f}{\partial \eta}e^{i\theta} - \frac{\partial f}{\partial \bar{\eta}}e^{-i\theta}\right).
\end{aligned} \tag{5}$$

Figure 2 shows the model of medium I bearing a line source force $\delta(\eta - \eta_0)$, with $\eta_0 = d + yi(y \le h)$ presenting the point on the vertical boundary.

The boundary condition of medium I can be expressed as follows:

$$\begin{cases}
\Gamma_{\mathrm{H}} \ : \ \tau_{yz}^{\mathrm{I}}\big|_{y=h} = 0,\ D_y^{\mathrm{I}}\big|_{y=h} = 0\\
\Gamma_{\mathrm{V}} : \ \tau_{xz}^{\mathrm{I}}\big|_{x=d} = \delta(\eta - \eta_0)\\
\Gamma_{\mathrm{C}} \ : \tau_{rz}^{\mathrm{I}}\big|_{r=a,-\pi\le\theta\le\pi} = 0\\
\Gamma_{\mathrm{C}} \ : \ G_\phi^{\mathrm{I}}\big|_{r=a,-\pi\le\theta\le\pi} = G_\phi^{c}\big|_{r=a,-\pi\le\theta\le\pi}\\
\Gamma_{\mathrm{C}} \ : D_r^{\mathrm{I}}\big|_{r=a,-\pi\le\theta\le\pi} = D_r^{c}\big|_{r=a,-\pi\le\theta\le\pi}
\end{cases} \tag{6}$$

where G_w^{I}, τ_{rz}^{I}, G_ϕ^{I} and D_r^{I} are anti-plane displacement, radial shear stress, electrical potential and electrical displacement, respectively; G_ϕ^c and D_r^c are the electrical potential and electrical displacement of the electrical field impacted by air in the circular cavity. $\delta(\square)$ is the Dirac-Delta function and G is the Green's function.

The essential solution has satisfied three conditions, including Eq. (6), the disturbance of the line source load $\delta(z - z_0)$, and the scattering displacement field due to the circular cavity. All of them could be regarded as the incident wave and the scattering wave, respectively. They also have satisfied both stress-free and electrical insulation conditions on the horizontal boundary. The incident wave can be expressed as follows by the mirror method and the multi-polar coordinate method:

$$G_w^i = \frac{i}{2c_{44}^{\mathrm{I}}(1+\lambda^{\mathrm{I}})}\left[H_0^{(1)}(k_1|\eta - \eta_0|) + H_0^{(1)}(k_1|\eta - \bar{\eta}_0 - 2hi|)\right], \quad G_\phi^i = \frac{e_{15}^{\mathrm{I}}}{\kappa_{11}^{\mathrm{I}}}G_w^i, \tag{7}$$

where $\lambda^{\mathrm{I}} = (e_{15}^{\mathrm{I}})^2/(c_{44}^{\mathrm{I}}\kappa_{11}^{\mathrm{I}})$ is the non-dimensional piezoelectric parameter.

The wave scattered by the circular cavity is reflected many times due to the boundary effect, with stress-free and electrical insulation conditions on the linear boundary of the right-angle space in medium I. It can be expressed as follows by the mirror method and the multi-polar coordinate method:

$$\begin{aligned} G_w^s &= \tfrac{i}{2c_{44}^{\mathrm{I}}(1+\lambda^{\mathrm{I}})} \sum_{n=-\infty}^{+\infty} A_n \sum_{j=1}^{4} S_n^{(j)},\ G_\phi^s = \tfrac{e_{15}^{\mathrm{I}}}{\kappa_{11}^{\mathrm{I}}} \left(G_w^s + f^s\right), \\ f^s &= \sum_{n=1}^{\infty} \left[B_n \sum_{j=1}^{4} \varphi_{1n}^{(j)} + C_n \sum_{j=1}^{4} \varphi_{2n}^{(j)} \right], \end{aligned} \tag{8}$$

where

$$\begin{aligned} S_n^{(1)} &= H_n^{(1)}(k_1 |\eta|)\,[\eta/|\eta|]^n\,, \\ S_n^{(2)} &= H_n^{(1)}(k_1 |\eta_1|)\,[\eta_1/|\eta_1|]^{-n}\,, \\ S_n^{(3)} &= (-1)^n H_n^{(1)}(k_1 |\eta_2|)\,[\eta_2/|\eta_2|]^n\,, \\ S_n^{(4)} &= (-1)^n H_n^{(1)}(k_1 |\eta_3|)\,[\eta_3/|\eta_3|]^{-n}\,, \\ \varphi_{1n}^{(1)} &= \eta^{-n}, \quad \varphi_{1n}^{(2)} = (\bar{\eta} + 2hi)^{-n}, \\ \varphi_{1n}^{(3)} &= (-1)^n(\bar{\eta} - 2d)^{-n}, \quad \varphi_{1n}^{(4)} = (-1)^n(\eta - 2d - 2hi)^{-n}, \\ \varphi_{2n}^{(1)} &= \bar{\eta}^{-n}, \quad \varphi_{2n}^{(2)} = (\eta - 2hi)^{-n}, \\ \varphi_{2n}^{(3)} &= (-1)^n(\eta - 2d)^{-n}, \quad \varphi_{2n}^{(4)} = (-1)^n(\bar{\eta} - 2d + 2hi)^{-n}, \\ \eta_1 &= \eta - 2hi, \quad \eta_2 = \eta_1 - 2d, \quad \eta_3 = \eta - 2d. \end{aligned}$$

The total Green's function of displacement and the total Green's function of the electrical potential for medium I can be expressed as follows:

$$G_w^{\mathrm{I}} = G_w^i + G_w^s, \quad G_\phi^{\mathrm{I}} = G_\phi^i + G_\phi^s \tag{9}$$

The expression of the electrical field in the cavity is:

$$G_\phi^c = \frac{e_{15}^c}{\kappa_{11}^c} f^c, \quad f^c = D_0 + \sum_{n=1}^{+\infty} (D_n \eta^n + E_n \bar{\eta}^n), \tag{10}$$

where A_n, B_n, C_n, D_n and E_n are unknown coefficients to be determined by the boundary conditions.

According to Eq. (6), the equations to determine the unknown quantities A_n, B_n, C_n, D_n and E_n are established as follows:

$$\begin{aligned} &\sum_{n=-\infty}^{+\infty} A_n \xi_n^{(11)} + \sum_{n=1}^{+\infty} B_n \xi_n^{(12)} + \sum_{n=1}^{+\infty} C_n \xi_n^{(13)} + \sum_{n=0}^{+\infty} D_n \xi_n^{(14)} + \sum_{n=1}^{+\infty} E_n \xi_n^{(15)} = \xi^{(1)}, \\ &\sum_{n=-\infty}^{+\infty} A_n \xi_n^{(21)} + \sum_{n=1}^{+\infty} B_n \xi_n^{(22)} + \sum_{n=1}^{+\infty} C_n \xi_n^{(23)} + \sum_{n=0}^{+\infty} D_n \xi_n^{(24)} + \sum_{n=1}^{+\infty} E_n \xi_n^{(25)} = \xi^{(2)}, \\ &\sum_{n=1}^{+\infty} B_n \xi_n^{(32)} + \sum_{n=1}^{+\infty} C_n \xi_n^{(33)} + \sum_{n=0}^{+\infty} D_n \xi_n^{(35)} + \sum_{n=1}^{+\infty} E_n \xi_n^{(36)} = \xi^{(3)}, \end{aligned} \tag{11}$$

where

$$\begin{aligned} \xi_n^{(11)} &= \frac{ik_1}{4} \left[\sum_{j=1}^{4} \chi_n^{(j)} \exp(i\theta) + \sum_{j=1}^{4} \gamma_n^{(j)} \exp(-i\theta) \right], \\ \xi_n^{(12)} &= \frac{(e_{15}^{\mathrm{I}})^2}{\kappa_{11}^{\mathrm{I}}} \left[\sum_{j=1}^{2} \varsigma_n^{(j)} \exp(i\theta) + \sum_{j=1}^{2} \vartheta_n^{(j)} \exp(-i\theta) \right], \end{aligned}$$

$$\xi_n^{(13)} = \frac{(e_{15}^{\mathrm{I}})^2}{\kappa_{11}^{\mathrm{I}}}\left[\sum_{j=1}^{2}\upsilon_n^{(j)}\exp(i\theta)+\sum_{j=1}^{2}\psi_n^{(j)}\exp(-i\theta)\right],$$

$$\xi_n^{(14)} = -\frac{(e_{15}^{c})^2}{\kappa_{11}^{c}}n\eta^n\exp(i\theta),\ \xi_n^{(15)} = -\frac{(e_{15}^{c})^2}{\kappa_{11}^{c}}n\bar{\eta}^n\exp(-i\theta),\ \xi_n^{(21)} = \frac{e_{15}^{\mathrm{I}}i}{2c_{44}^{\mathrm{I}}(1+\lambda^{\mathrm{I}})\kappa_{11}^{\mathrm{I}}}\sum_{j=1}^{4}S_n^{(j)},$$

$$\xi_n^{(22)} = \frac{e_{15}^{\mathrm{I}}}{\kappa_{11}^{\mathrm{I}}}\sum_{j=1}^{4}\varphi_{1n}^{(j)},\ \xi_n^{(23)} = \frac{e_{15}^{\mathrm{I}}}{\kappa_{11}^{\mathrm{I}}}\sum_{j=1}^{4}\varphi_{2n}^{(j)},\ \xi_n^{(24)} = -\frac{e_{15}^{c}}{\kappa_{11}^{c}}\eta^n,\ \xi_n^{(25)} = -\frac{e_{15}^{c}}{\kappa_{11}^{c}}\bar{\eta}^n,$$

$$\xi_n^{(32)} = -e_{15}^{\mathrm{I}}\left[\sum_{j=1}^{2}\varsigma_n^{(j)}\exp(i\theta)+\sum_{j=1}^{2}\vartheta_n^{(j)}\exp(-i\theta)\right],$$

$$\xi_n^{(33)} = -e_{15}^{\mathrm{I}}\left[\sum_{j=1}^{2}\upsilon_n^{(j)}\exp(i\theta)+\sum_{j=1}^{2}\psi_n^{(j)}\exp(-i\theta)\right],$$

$$\xi_n^{(34)} = e_{15}^{c}n\eta^{n-1}\exp(i\theta),\ \xi_n^{(35)} = e_{15}^{c}n\bar{\eta}^{n-1}\exp(-i\theta),$$

$$\begin{aligned}\xi^{(1)} = -\tfrac{ik_1}{4}\Big\{&\Big[H_{-1}^{(1)}(k_1|\eta-\eta_0|)\tfrac{\bar{\eta}-\bar{\eta}_0}{|\eta-\eta_0|}+\ H_{-1}^{(1)}(k_1|\eta-\bar{\eta}_0-2hi|)\tfrac{\bar{\eta}-\eta_0+2hi}{|\eta-\bar{\eta}_0-2hi|}\Big]e^{i\theta}\\&+\Big[H_{-1}^{(1)}(k_1|\eta-\eta_0|)\tfrac{\eta-\eta_0}{|\eta-\eta_0|}+\ H_{-1}^{(1)}(k_1|\eta-\bar{\eta}_0-2hi|)\tfrac{\eta-\bar{\eta}_0-2hi}{|\eta-\bar{\eta}_0-2hi|}\Big]e^{-i\theta}\Big\},\end{aligned}$$

$$\xi^{(2)} = -\frac{ie_{15}^{\mathrm{I}}}{2c_{44}^{\mathrm{I}}(1+\lambda^{\mathrm{I}})\kappa_{11}^{\mathrm{I}}}\left[H_0^{(1)}(k_1|\eta-\eta_0|)+\ H_0^{(1)}(k_1|\eta-\bar{\eta}_0-2hi|)\right],$$

$$\xi^{(3)} = 0$$

$$\chi_n^{(1)} = H_{n-1}^{(1)}(k_1|\eta|)\,[\eta/|\eta|]^{n-1},\quad \chi_n^{(2)} = -H_{n+1}^{(1)}(k_1|\eta_1|)\,[\eta_1/|\eta_1|]^{-n-1},$$

$$\chi_n^{(3)} = (-1)^n H_{n-1}^{(1)}(k_1|\eta_2|)\,[\eta_2/|\eta_2|]^{n-1},$$

$$\chi_n^{(4)} = -(-1)^n H_{n+1}^{(1)}(k_1|\eta_3|)\,[\eta_3/|\eta_3|]^{-n-1},$$

$$\gamma_n^{(1)} = -H_{n+1}^{(1)}(k_1|\eta|)\,[\eta/|\eta|]^{n+1},\quad \gamma_n^{(2)} = H_{n-1}^{(1)}(k_1|\eta_1|)\,[\eta_1/|\eta_1|]^{-n+1},$$

$$\gamma_n^{(3)} = -(-1)^n H_{n+1}^{(1)}(k_1|\eta_2|)\,[\eta_2/|\eta_2|]^{n+1},$$

$$\gamma_n^{(4)} = (-1)^n H_{n-1}^{(1)}(k_1|\eta_3|)\,[\eta_3/|\eta_3|]^{-n+1},$$

$$\varsigma_n^{(1)} = -n\eta^{-n-1},\quad \varsigma_n^{(2)} = -(-1)^n n(\eta-2d-2hi)^{-n-1},$$

$$\vartheta_n^{(1)} = -n(\bar{\eta}+2hi)^{-n-1},\quad \vartheta_n^{(2)} = -(-1)^n n(\bar{\eta}-2d)^{-n-1},$$

$$\upsilon_n^{(1)} = -n(\eta-2hi)^{-n-1},\quad \upsilon_n^{(2)} = -n(-1)^n(\eta-2d)^{-n-1},$$

$$\psi_n^{(1)} = -n\bar{\eta}^{-n-1},\quad \psi_n^{(2)} = -(-1)^n n(\bar{\eta}-2d+2hi)^{-n-1}.$$

In order to solve Eq. (11), both sides are multiplied by $\exp(-im\theta)$, $(m = 0, \pm1, \pm2\cdots)$. Corresponding to the interval $(-\pi, \pi)$, the equation is determined and integrated as well. Next, a series of algebraic equations is obtained:

$$\sum_{n=-\infty}^{+\infty}A_n\xi_{mn}^{(11)}+\sum_{n=1}^{+\infty}B_n\xi_{mn}^{(12)}+\sum_{n=1}^{+\infty}C_n\xi_{mn}^{(13)}+\sum_{n=0}^{+\infty}D_n\xi_{mn}^{(14)}+\sum_{n=1}^{+\infty}E_n\xi_{mn}^{(15)} = \xi_m^{(1)},$$

$$\sum_{n=-\infty}^{+\infty}A_n\xi_{mn}^{(21)}+\sum_{n=1}^{+\infty}B_n\xi_{mn}^{(22)}+\sum_{n=1}^{+\infty}C_n\xi_{mn}^{(23)}+\sum_{n=0}^{+\infty}D_n\xi_{mn}^{(24)}+\sum_{n=1}^{+\infty}E_n\xi_{mn}^{(25)} = \xi_m^{(2)},$$

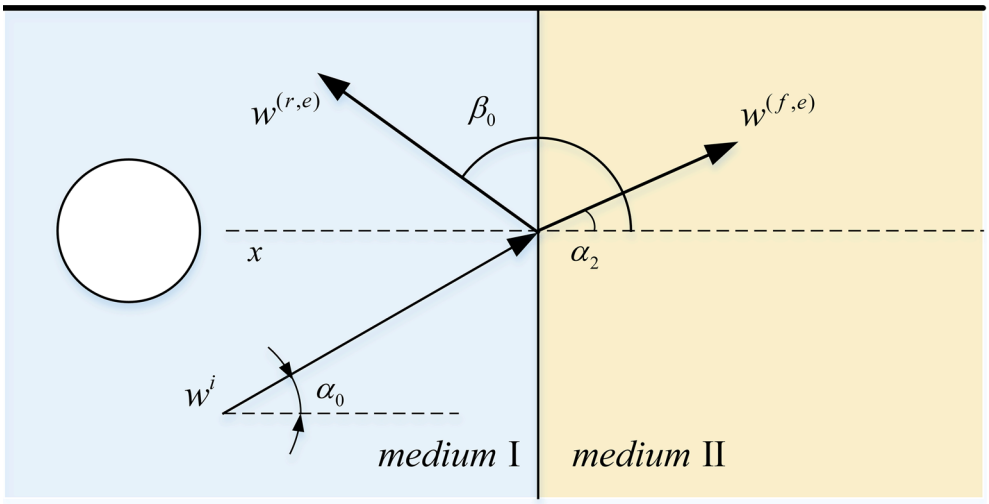

Fig. 3 Reflected and refracted waves caused by interface

$$\sum_{n=1}^{+\infty} B_n \xi_{mn}^{(32)} + \sum_{n=1}^{+\infty} C_n \xi_{mn}^{(33)} + \sum_{n=0}^{+\infty} D_n \xi_{mn}^{(35)} + \sum_{n=1}^{+\infty} E_n \xi_{mn}^{(36)} = \xi_m^{(3)}, \tag{12}$$

where

$$\xi_{mn}^{(11)} = \int_{-\pi}^{\pi} \xi_n^{(11)} e^{-im\theta} d\theta, \quad \xi_{mn}^{(12)} = \int_{-\pi}^{\pi} \xi_n^{(12)} e^{-im\theta} d\theta, \quad \xi_{mn}^{(13)} = \int_{-\pi}^{\pi} \xi_n^{(13)} e^{-im\theta} d\theta, \quad \xi_{mn}^{(14)} = \int_{-\pi}^{\pi} \xi_n^{(14)} e^{-im\theta} d\theta,$$
$$\xi_{mn}^{(15)} = \int_{-\pi}^{\pi} \xi_n^{(15)} e^{-im\theta} d\theta, \quad \xi_{mn}^{(21)} = \int_{-\pi}^{\pi} \xi_n^{(21)} e^{-im\theta} d\theta, \quad \xi_{mn}^{(22)} = \int_{-\pi}^{\pi} \xi_n^{(22)} e^{-im\theta} d\theta, \quad \xi_{mn}^{(23)} = \int_{-\pi}^{\pi} \xi_n^{(23)} e^{-im\theta} d\theta,$$
$$\xi_{mn}^{(24)} = \int_{-\pi}^{\pi} \xi_n^{(24)} e^{-im\theta} d\theta, \quad \xi_{mn}^{(25)} = \int_{-\pi}^{\pi} \xi_n^{(25)} e^{-im\theta} d\theta, \quad \xi_{mn}^{(32)} = \int_{-\pi}^{\pi} \xi_n^{(32)} e^{-im\theta} d\theta, \quad \xi_{mn}^{(33)} = \int_{-\pi}^{\pi} \xi_n^{(33)} e^{-im\theta} d\theta,$$
$$\xi_{mn}^{(35)} = \int_{-\pi}^{\pi} \xi_n^{(35)} e^{-im\theta} d\theta, \quad \xi_{mn}^{(36)} = \int_{-\pi}^{\pi} \xi_n^{(36)} e^{-im\theta} d\theta, \quad \xi_m^{(1)} = \int_{-\pi}^{\pi} \xi^{(1)} e^{-im\theta} d\theta, \quad \xi_m^{(2)} = \int_{-\pi}^{\pi} \xi^{(2)} e^{-im\theta} d\theta,$$
$$\xi_m^{(3)} = 0.$$

The Green's function for medium II can be expressed as follows:

$$G_w^{\mathrm{I}} = \frac{i}{2c_{44}^{\mathrm{I}}(1+\lambda^{\mathrm{I}})} \left[H_0^{(1)}(k_2 |\eta - \eta_0|) + H_0^{(1)}(k_2 |\eta - \bar{\eta}_0 - 2hi|) \right], \quad G_\phi^{\mathrm{I}} = \frac{e_{15}^{\mathrm{I}}}{\kappa_{11}^{\mathrm{I}}} G_w^{\mathrm{I}}. \tag{13}$$

4 Scattering of SH-wave

A well-bonded piezoelectric bi-material with a cavity and cracks is subjected to an incident SH-wave in this section. Figure 3 shows the reflected and refracted waves caused by the interface.

The boundary conditions of the well-bonded piezoelectric bi-material are:

(1) The two cracks are assumed to be stress-free and electrically permeable.
(2) The electro-elastic fields are continuous at the well-bonded linking section outside the crack of the bi-material media.

It is difficult to obtain the expression of the incident elastic displacement w^i and incident electrical potential ϕ^i, which satisfies stress-free and electrical insulation conditions on the horizontal boundary and the continuity condition for the SH-wave on the vertical boundary. In order to overcome these difficulties, the mirror method which can transform the right-angle space to the global space, and the multi-polar coordinate method are used.

According to references [3,4,11,15], the equivalent incident wavew^i and the corresponding electrical potential ϕ^i can be expressed as follows, respectively:

$$\begin{aligned} w^i &= w_0 \left\{ \exp\left\{ \tfrac{ik_1}{2} \left[(\eta - d - hi)e^{-i\alpha_0} + (\bar{\eta} - d + hi)e^{i\alpha_0} \right] \right\} \right. \\ &\quad \left. + \exp\left\{ \tfrac{ik_1}{2} \left[(\eta - d - hi)e^{i\alpha_0} + (\bar{\eta} - d + hi)e^{-i\alpha_0} \right] \right\} \right\}, \\ \phi^i &= \phi_0 \left\{ \exp\left\{ \tfrac{ik_1}{2} \left[(\eta - d - hi)e^{-i\alpha_0} + (\bar{\eta} - d + hi)e^{i\alpha_0} \right] \right\} \right. \\ &\quad \left. + \exp\left\{ \tfrac{ik_1}{2} \left[(\eta - d - hi)e^{i\alpha_0} + (\bar{\eta} - d + hi)e^{-i\alpha_0} \right] \right\} \right\}. \end{aligned} \tag{14}$$

Similarly, the equivalent reflected wave w^r and the corresponding electrical potential ϕ^r are:

$$\begin{aligned} w^r &= w_1 \left\{ \exp\left\{ \tfrac{ik_1}{2} \left[(\eta - d - hi)e^{-i\beta} + (\bar{\eta} - d + hi)e^{i\beta} \right] \right\} \right. \\ &\quad \left. + \exp\left\{ \tfrac{ik_1}{2} \left[(\eta - d - hi)e^{i\beta} + (\bar{\eta} - d + hi)e^{-i\beta} \right] \right\} \right\}, \\ \phi^r &= \phi_1 \left\{ \exp\left\{ \tfrac{ik_1}{2} \left[(\eta - d - hi)e^{-i\beta} + (\bar{\eta} - d + hi)e^{i\beta} \right] \right\} \right. \\ &\quad \left. + \exp\left\{ \tfrac{ik_1}{2} \left[(\eta - d - hi)e^{i\beta} + (\bar{\eta} - d + hi)e^{-i\beta} \right] \right\} \right\}. \end{aligned} \tag{15}$$

The equivalent refracting wavew^f and the corresponding electrical potentialϕ^f are:

$$\begin{aligned} w^f &= w_2 \left\{ \exp\left\{ \tfrac{ik_2}{2} \left[(\eta - d - hi)e^{-i\alpha_2} + (\bar{\eta} - d + hi)e^{i\alpha_2} \right] \right\} \right. \\ &\quad \left. + \exp\left\{ \tfrac{ik_2}{2} \left[(\eta - d - hi)e^{i\alpha_2} + (\bar{\eta} - d + hi)e^{-i\alpha_2} \right] \right\} \right\}, \\ \phi^f &= \phi_2 \left\{ \exp\left\{ \tfrac{ik_2}{2} \left[(\eta - d - hi)e^{-i\alpha_2} + (\bar{\eta} - d + hi)e^{i\alpha_2} \right] \right\} \right. \\ &\quad \left. + \exp\left\{ \tfrac{ik_2}{2} \left[(\eta - d - hi)e^{i\alpha_2} + (\bar{\eta} - d + hi)e^{-i\alpha_2} \right] \right\} \right\}, \end{aligned} \tag{16}$$

where $\beta_0 = \pi - \alpha_0$, $\alpha_0$is the incident angle, α_2 is the refracted angle, and the relationship of the parameters above can be expressed as follows:

$$\begin{cases} w_0 + w_1 = w_2, \\ \phi_0 + \phi_1 = \phi_2, \\ k_1 \sin\alpha_0 = k_2 \sin\alpha_2. \end{cases} \tag{17}$$

Thus, Eqs. (15)–(17) satisfy the continuity condition on the vertical boundary Γ_V:

$$\begin{cases} w^i + w^r = w^f, \\ \phi^i + \phi^r = \phi^f, \end{cases} \tag{18}$$

$$\begin{aligned} w^s &= \tfrac{i}{2c_{44}^{\mathrm{I}}(1+\lambda^{\mathrm{I}})} \sum_{n=-\infty}^{+\infty} K_n \sum_{j=1}^{4} S_n^{(j)}, \quad \phi^s = \tfrac{e_{15}^{\mathrm{I}}}{\kappa_{11}^{\mathrm{I}}} \left(w^s + f_w^s \right), \\ f_w^s &= \sum_{n=1}^{\infty} \left[L_n \sum_{j=1}^{4} \varphi_{1n}^{(j)} + P_n \sum_{j=1}^{4} \varphi_{2n}^{(j)} \right], \\ \phi^c &= \frac{e_{15}^c}{\kappa_{11}^c} f_w^c, \quad f_w^c = R_0 + \sum_{n=1}^{+\infty} (R_n \eta^n + T_n \bar{\eta}^n). \end{aligned} \tag{19}$$

The expression of the scattering wave and the standing wave by SH-wave are the same as those produced by the Green's function. The integral equations are constructed to determine the unknown quantities such as K_n, L_n, P_n, R_n and T_n from the boundary condition, just like Eq. (6). In which, determined coefficients are the same as those in Eq. (12). The solution process is similar to the method to solve Green's function.

As Fig. 4 shows, the conjunction method and the crack-division technique are used in order to obtain the expression of the displacement field and electric field from the SH-wave. According to references [15–17],

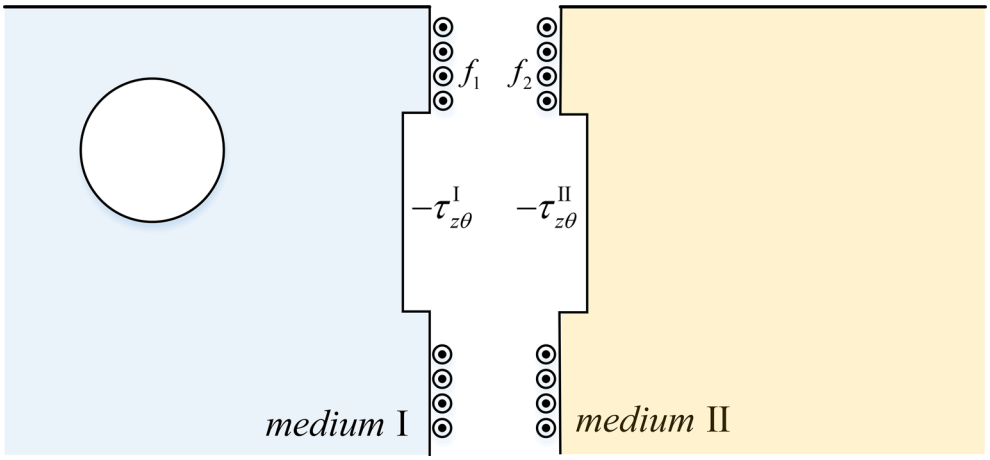

Fig. 4 Conjunction of piezoelectric bi-material half-space with a circular cavity and an interface crack

the bi-material half-space is divided into two parts along the vertical boundary based on the assumption of stress-free and electrical permeable cracks. Then, a pair of unknown anti-plane forces $f_1(r'_0, \theta'_0)$ and $f_2(r'_0, \theta'_0)$ is applied on the left (or right) section of the vertical boundary outside the crack, respectively, to satisfy the continuity condition of stress and displacement on the vertical boundary outside the crack. Meanwhile, a pair of anti-plane forces is defined as $\tau^{\mathrm{I}}_{z\theta}$ and $\tau^{\mathrm{II}}_{z\theta}$, respectively, and in opposite direction to each other. So, the residual force is zero and the electrical field is continuous on the left (or right) section of the region which can be thought of as the permeable crack. According to the continuity conditions, the first kind of Fredholm integral equations containing undetermined anti-plane forces is established, where r'_0 and θ'_0 are the polar coordinates at the linking sections in the local coordinate system $x'o'y'$, when $\theta'_0 = \beta_1 = \pi/2$, $A \le r'_0 \le A + h_1$, when $\theta'_0 = \beta_2 = -\pi/2$, $A \le r'_0 \le \infty$.

The total displacements W^{I}, W^{II} and the total stresses $\tau^{\mathrm{I}}_{\theta z}$, $\tau^{\mathrm{II}}_{\theta z}$ at the linking sections are:

$$\begin{aligned} &W^{\mathrm{I}} = w^i + w^r + w^s, \quad \tau^{\mathrm{I}}_{\theta z} = \tau^i_{\theta z} + \tau^r_{\theta z} + \tau^s_{\theta z}, \\ &W^{\mathrm{II}} = w^f, \quad \tau^{\mathrm{II}}_{\theta z} = \tau^f_{\theta z}. \end{aligned} \tag{20}$$

The displacement continuity conditions at the interface can be expressed as:

$$W^{\mathrm{I}} + w^{f1} + w^{c1} = W^{\mathrm{II}} + w^{f2} + w^{c2}. \tag{21}$$

According to $w^i + w^r = w^f$ we can obtain

$$w^s + w^{f1} + w^{c1} = w^{f2} + w^{c2}, \tag{22}$$

where w^{f1} is the displacement field on the vertical boundary and produced by the anti-plane external force system $f_1(r'_0, \theta'_0)$ acting on the vertical boundary of medium I. w^{f2} is the displacement field on the vertical boundary and produced by the anti-plane external force system $f_2(r'_0, \theta'_0)$ acting on the vertical boundary of medium I. w^{c1} is the displacement field on the vertical boundary and produced by the anti-plane external force system $-\tau^{\mathrm{I}}_{z\theta}$ acting on the region where crack appear in medium I. $w^{c2}$is the displacement field on the vertical boundary and produced by the anti-plane external force system $-\tau^{\mathrm{II}}_{z\theta}$ acting on the region where the crack appears in medium II. The expression of w^{f1}, w^{f2}, w^{c1} and w^{c2} can be written as follows:

$$\begin{aligned} w^{f1} &= \int_A^{A+h_1} f_1(r'_0, \beta_1) G^{\mathrm{I}}_w(r'_0, \beta_1; r', \theta') dr'_0 + \int_A^{\infty} f_1(r'_0, \beta_2) G^{\mathrm{I}}_w(r'_0, \beta_2; r', \theta') dr'_0, \\ w^{f2} &= -\int_A^{A+h_1} f_2(r'_0, \beta_1) G^{\mathrm{II}}_w(r'_0, \beta_1; r', \theta') dr'_0 - \int_A^{\infty} f_2(r'_0, \beta_2) G^{\mathrm{II}}_w(r'_0, \beta_2; r', \theta') dr'_0, \\ w^{c1} &= -\int_0^{A} \tau^{\mathrm{I}}_{\theta z}(r'_0, \beta_1) G^{\mathrm{I}}_w(r'_0, \beta_1; r', \theta') dr'_0 + \int_0^{A} \tau^{\mathrm{I}}_{\theta z}(r'_0, \beta_2) G^{\mathrm{I}}_w(r'_0, \beta_2; r', \theta') dr'_0, \\ w^{c2} &= \int_0^{A} \tau^{\mathrm{II}}_{\theta z}(r'_0, \beta_1) G^{\mathrm{II}}_w(r'_0, \beta_1; r', \theta') dr'_0 - \int_0^{A} \tau^{\mathrm{II}}_{\theta z}(r'_0, \beta_2) G^{\mathrm{II}}_w(r'_0, \beta_2; r', \theta') dr'_0. \end{aligned} \tag{23}$$

The stress continuity conditions at the linking section can be expressed as:

$$\tau_{\theta z}^{\mathrm{I}} \sin\theta_0' + f_1(r_0', \theta_0') = \tau_{\theta z}^{\mathrm{II}} \sin\theta_0' + f_2(r_0', \theta_0'). \tag{24}$$

According to $\tau_{xz}^{i} + \tau_{xz}^{r} = \tau_{xz}^{f}$, we get

$$f_1(r_0', \quad \theta_0') = f_2(r_0', \theta_0'), \quad \theta_0' = \beta_1, \quad \beta_2. \tag{25}$$

The integral equations containing the unknown anti-plane forces are established as:

$$\begin{aligned}
&f_1(r_0', \theta_0') = f_2(r_0', \theta_0'), \quad \theta_0' = \beta_1, \beta_2; \\
&\textstyle\int_A^{A+h_1} f_1(r_0', \beta_1)\left[G_w^{\mathrm{I}}(r_0', \beta_1; r', \theta') + G_w^{\mathrm{I}}(r_0', \beta_1; r', \theta')\right] dr_0' \\
&\quad + \textstyle\int_A^{\infty} f_1(r_0', \beta_2)\left[G_w^{\mathrm{II}}(r_0', \beta_2; r', \theta') + G_w^{\mathrm{I}}(r_0', \beta_2; r', \theta')\right] dr_0' \\
&\quad = -w^s + \textstyle\int_0^A \tau_{\theta z}^{\mathrm{II}}(r_0', \beta_1) G_w^{\mathrm{I}}(r_0', \beta_1; r', \theta') dr_0' \\
&\quad - \textstyle\int_0^A \tau_{\theta z}^{\mathrm{I}}(r_0', \beta_2) G_w^{\mathrm{I}}(r_0', \beta_2; r', \theta') dr_0' \\
&\quad + \textstyle\int_0^A \tau_{\theta z}^{\mathrm{II}}(r_0', \beta_1) G_w^{\mathrm{II}}(r_0', \beta_1; r', \theta') dr_0' \\
&\quad - \textstyle\int_0^A \tau_{\theta z}^{\mathrm{II}}(r_0', \beta_2) G_w^{\mathrm{II}}(r_0', \beta_2; r', \theta') dr_0'.
\end{aligned} \tag{26}$$

The integral equations above are Fredholm equations of the first kind. When the mirror point and source point of the Green's function coincide, there is a singularity from the logarithm in the Fredholm equations. According to the attenuation characteristic of Green's function and the scattering wave, Eq. (26) could be converted to algebraic equations by a direct discrete method, and the unknown forces $f_1(r_0', \theta_0')$ and $f_2(r_0', \theta_0')$ could be determined at a series of discrete points.

5 Dynamic stress concentration factor (DSCF)

The circumferential shear stresses around the cylindrical cavity can be expressed as follows:

$$\tau_{\theta z} = \tau_{\theta z}^{\mathrm{I}} + \int_A^{A+h_1} f_1(r_0', \beta_1) \frac{\mu_1}{r_0'} \frac{\partial G_w^{\mathrm{I}}(r_0', \beta_1; r', \theta')}{\partial \theta'} dr_0' + \int_A^{\infty} f_1(r_0', \beta_2) \frac{\mu_1}{r_0'} \frac{\partial G_w^{\mathrm{I}}(r_0', \beta_2; r', \theta')}{\partial \theta'} dr_0'. \tag{27}$$

The dynamic stress concentration factor (DSCF) can be expressed as

$$\tau_{\theta z}^{*} = \left|\tau_{\theta z}/\tau_0\right|, \tag{28}$$

where $\tau_0 = ik_1\mu_1 w_0$ is amplitude of the shear stress induced by the incident wave.

6 Dynamic stress intensity factor (DSIF)

The external force system $f_1(r_0', \theta_0')$ has a singularity of the square root at the crack tip, so the dynamic stress intensity factor is introduced as:

$$k_{III} = \lim_{r_0' \to A} f_1(r_0', \theta_0') \cdot \sqrt{2(r_0' - A)}. \tag{29}$$

In order to make Eq. (26) include the dynamic stress intensity factor k_{III} directly, the integrand function can be transformed as follows:

$$f_1\left(G_w^{\mathrm{I}} + G_w^{\mathrm{II}}\right) = \left[\lim_{r_0' \to A} f_1 \cdot \sqrt{2(r_0' - A)}\right] \cdot \left[\left(G_w^{\mathrm{I}} + G_w^{\mathrm{II}}\right) / \sqrt{2(r_0' - A)}\right]. \tag{30}$$

The value at the crack tip is the dynamic stress intensity factor k_I from solving the transformed equation (26). The non-dimensional dynamic stress intensity factor is defined as:

$$k_3 = \left|\frac{k_{III}}{(\tau_0 Q)}\right|, \tag{31}$$

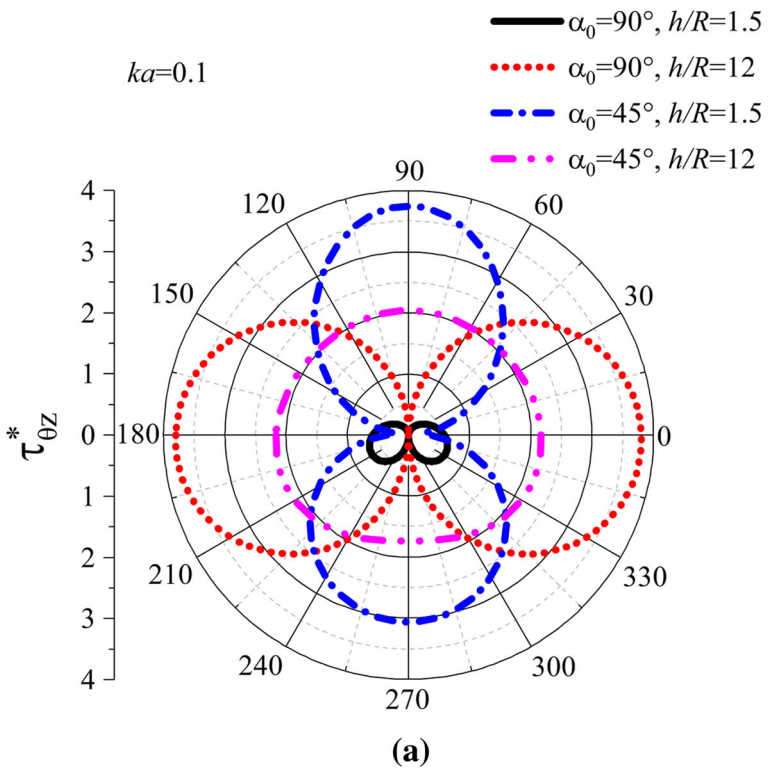

(a)

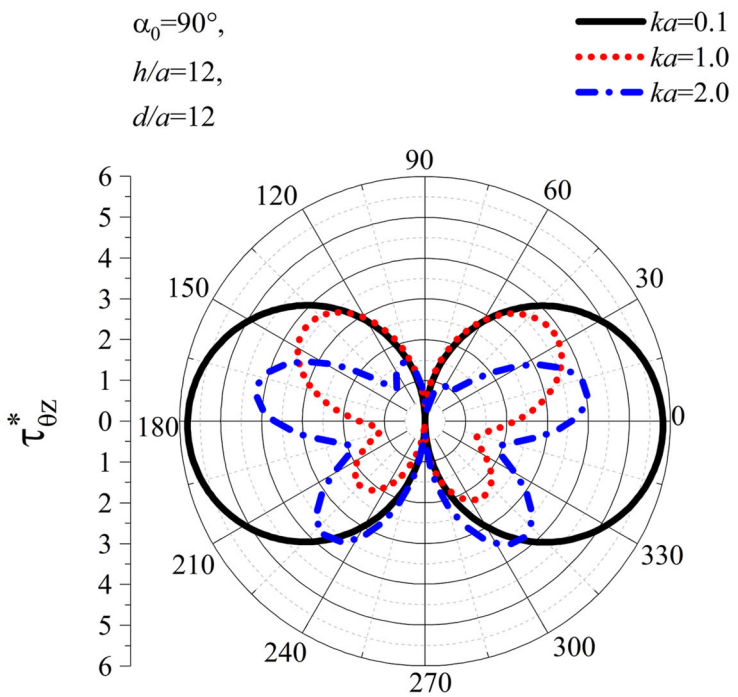

(b)

Fig. 5 The verification of the method presented in this paper

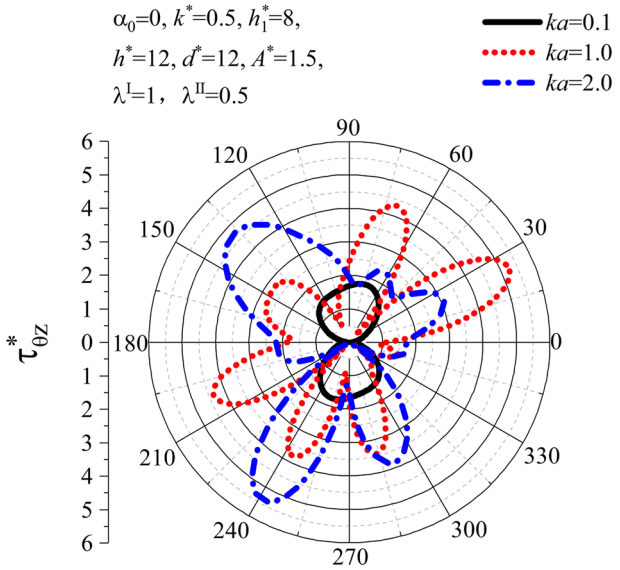

Fig. 6 Distribution of DSCF around circular cavity edge vs. ka by horizontal SH-wave

where Q is a characteristic parameter with dimension of square of length.

As illustrated above, the dynamic stress concentration factor (DSCF) around the cylindrical inclusion and the dynamic stress intensity factor (DSIF) at the crack tip are given. The effects of free boundary, vertical interface, length of crack and different combinations of material parameters are discussed. Here, the dimensionless parameters are $k_1 = k$, $k^* = k_2/k_1$, $h^* = h/a$, $h_1^* = h_1/a$, $d^* = d/a$ and $A^* = A/a$.

Figure 5a gives the distribution of the dynamic stress concentration factor (DSCF) around the cylindrical cavity disturbed by the SH-wave under the extreme condition of $\lambda^{\mathrm{I}} = \lambda^{\mathrm{II}} = 0$, $c_{44}^{\mathrm{I}} = c_{44}^{\mathrm{II}}$, $\rho_1 = \rho_2$, $k_1 = k_2$ and $A = 0$. The effect of the crack is ignored, and the numerical examples in this paper could degenerate to the case of a cylindrical hole in an elastic half space, which is the case of reference [18]. Figure 5b gives the variation of the dynamic stress concentration factor (DSCF) around the cylindrical cavity disturbed by the SH-wave under the extreme condition of $\lambda^{\mathrm{I}} = \lambda^{\mathrm{II}} = 0$, $c_{44}^{\mathrm{II}} = 0$, $k_2 = 0$, $\rho_2 = 0$ and $A = 0$. In this situation, the crack is ignored, and the numerical examples in this paper can degenerate to the case of a cylindrical hole in an elastic quarter space, which is reported in reference [6]. When the combined parameters of references [6,18] are applied in this study, those newly obtained results are in good agreement with the previous report. So, the methods used in this investigation are fully verified.

Figure 6 gives the distribution of the dynamic stress concentration factor (DSCF) around the circular cavity disturbed by the horizontal SH-wave when the incident wave frequency ka has different values. When $ka = 0.1$, that is the "quasi-static" case, the graphic is almost symmetric, the maximum of DSCF is 2.8, at the point $\theta = 93°$. However, the change of the DSCF is obvious in the middle and high frequency range. When $ka = 2$, the value of the DSCF reaches the maximum of 5.7 ($\theta = -118°$), and this value is about twice the one in the "quasi-static" case. So, the incident wave frequency ka should not be ignored. The larger the frequency is, the more obvious the effect of the interface would be.

Figure 7 gives the variation of the dynamic stress concentration factor (DSCF) around the circular cavity disturbed by the SH-wave with various incidence angles. When the incident wave is horizontal or vertical, the value of the DSCF is much larger than at oblique angle. The maximum is in the upper and lower region of the circular cavity when the incident wave is vertical, while the maximum is in the left and right region of the circular cavity when the incident wave is horizontal. When the incident wave in the "quasi-static" case is vertical, the value of the DSCF reaches the maximum of 2 ($\theta = 0°$). Compared with the case of horizontal incident wave, this value is increased by more than 1.6 times.

Figures 8 and 9 give the distribution of the dynamic stress concentration factor (DSCF) around the circular cavity varying with the non-dimensional piezoelectric parameters λ^{I} and λ^{II}, respectively, under the incidence of horizontal SH-wave. We find that the larger λ^{I} is, the higher the DSCF and the larger λ^{II} is, the lower the DSCF. When $\lambda^{\mathrm{II}} = 0.3$, the value of the DSCF reaches the maximum of 6.91 ($\theta = -119°$). Compared

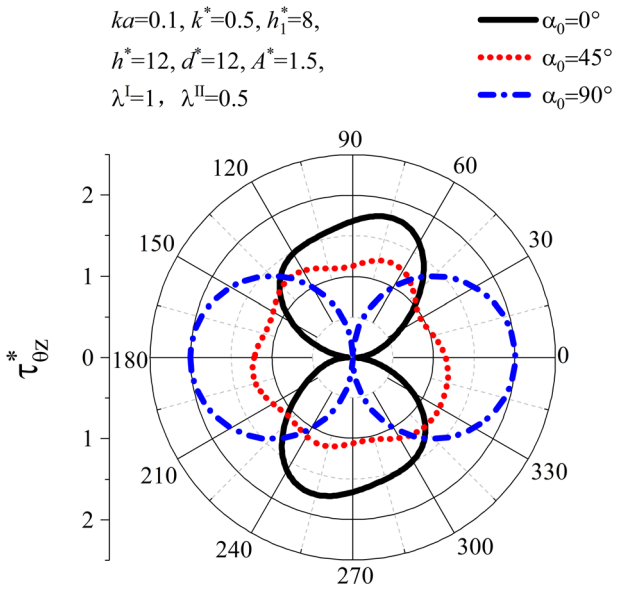

Fig. 7 Variation of DSCF around circular cavity edge by SH-wave with different incident angles

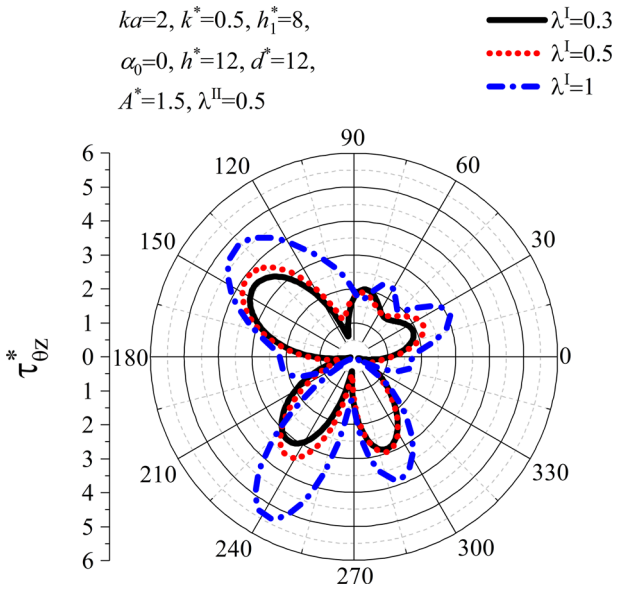

Fig. 8 Distribution of DSCF around circular cavity edge vs λ^{I} under horizontal incidence of SH-wave

with the maximum in the case of $\lambda^{\mathrm{I}} = 1$, this value is increased by more than 24.8%. So, the effect of the non-dimensional piezoelectric parameter is essential and the influence of λ^{II} is more obvious than that of λ^{I}.

Figure 10 gives the variation of the dynamic stress concentration factor (DSCF) around the circular cavity disturbed by the horizontal SH-wave, when k^* has different values. So, the larger k^* is, the smaller the value of the DSCF would be. That is because the soft medium can absorb part of the energy. When $k^* = 0.5$, the value of the DSCF reaches the maximum of 5.3 ($\theta = -119°$). Compared with the case of incident wavenumber ratio $k^* = 2$, this value is increased by more than 1.8 times.

Figure 11 gives the distribution of the dynamic stress concentration factor (DSCF) around the circular cavity varying with A^* under horizontal incidence of the SH-wave. The larger A^* is, the larger the value of the DSCF is. When $A^* = 2$, the value of the DSCF reaches the maximum of 3.1 ($\theta = 143°$). Compared with the case of $A^* = 1$, this value is increased by more than 1.7 times.

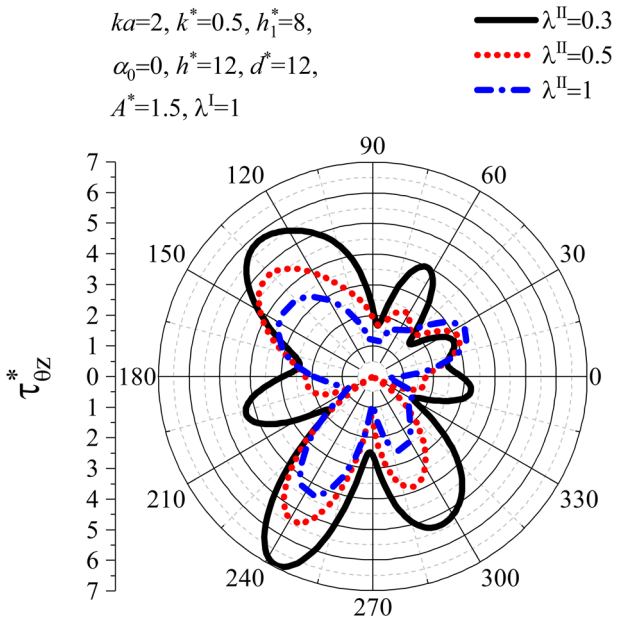

Fig. 9 Distribution of DSCF around circular cavity edge vs. λ^{II} under horizontal incidence of SH-wave

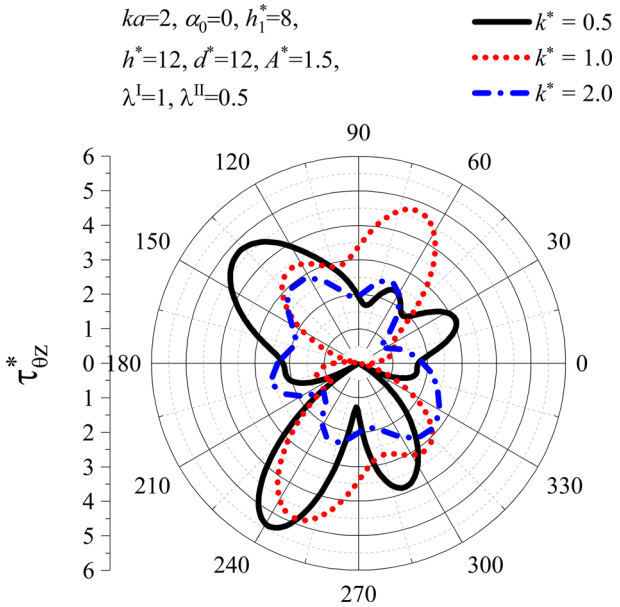

Fig. 10 Variation of DSCF around circular cavity edge vs. k^* by horizontal SH-wave

Figure 12 gives the variation of the dynamic stress intensity factor (DSIF) at the crack tip disturbed by the horizontal SH-wave when the non-dimensional piezoelectric parameter λ^{I} has different values. We can find that the larger value of λ^{I}, the smaller the value of the DSIF is. The graphic is pulsating and first increases, then decreases and finally increases. When $\lambda^{\mathrm{I}} = 0.3$ and $ka = 1.7$, the value of the DSIF reaches the maximum of 2.2.

Figure 13 gives the distribution of the dynamic stress intensity factor (DSIF) at the crack tip varying with A^* under horizontal incidence of the SH-wave. We could find that the larger A^* is, the higher the DSIF. The graphic is pulsating and first increases, then reduces and finally increases. When the crack length $A^* = 2$ and $ka = 1.6$, the value of the DSIF reaches the maximum of 1.3.

The physical meaning of the results is significant. The dynamic stress concentration factor indicates the possibility of damage in the region around the circular cavity. The larger the dynamic stress concentration

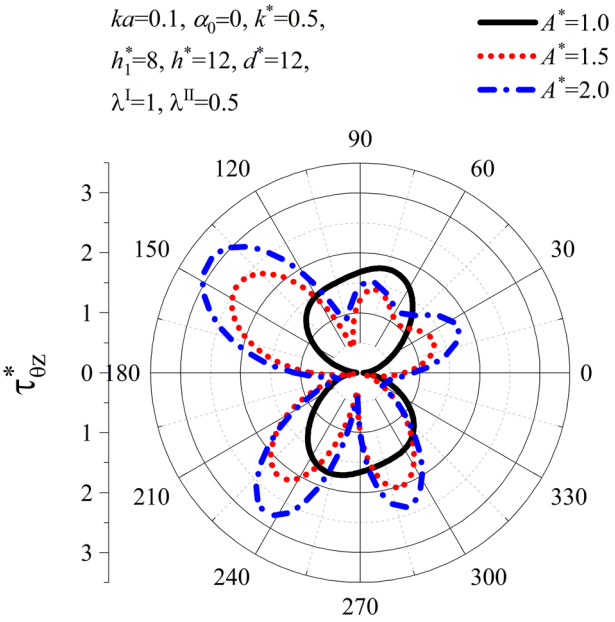

Fig. 11 Distribution of DSCF around circular cavity edge vs. A^* under horizontal incidence SH-wave

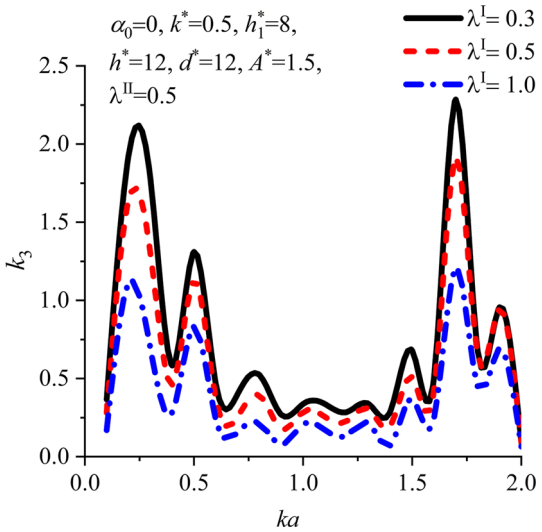

Fig. 12 Variation of DSIF at crack tip vs. λ^{I} by horizontal SH-wave

factor is, the higher the probability of damage is, and cracks will appear around the cavity if the dynamic stress concentration factor is large enough. The dynamic stress intensity factor indicates the possibility of crack propagation along the linking section of the piezoelectric bi-material. The larger dynamic stress intensity factor is, the larger the probability of crack propagation. If the dynamic stress intensity factor is large enough, those cracks would expand along the vertical boundary to cause facture. So, the dynamic stress concentration factor and dynamic stress intensity factor reflect the reliability of the piezoelectric bi-material and the possibility of fracture of structure.

As Table 1 shows, several specific combinations of physical parameters of the piezoelectric bi-material are obtained by numerical examples in which the constant parameters are $h_1^* = 8$, $h^* = 12$ and $d^* = 12$. If the ratio of the parameters is the same as the ratio in Table 1, the maximum of the dynamic stress concentration factor and the dynamic stress intensity factor can be locked up, so Table 1 provides a reference for practical engineering.

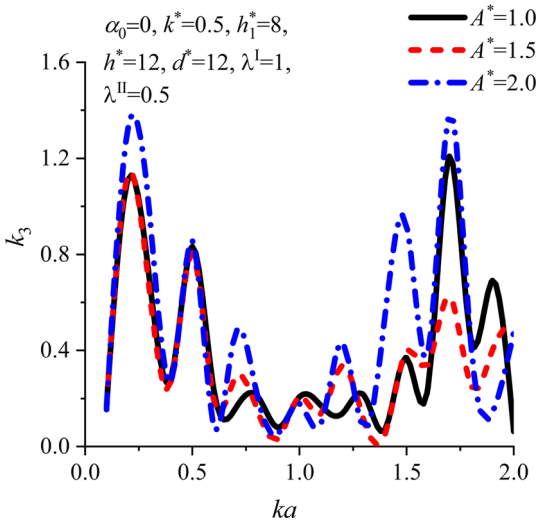

Fig. 13 Distribution of DSIF at crack tip vs. A^* under horizontal incidence of SH-wave

Table 1 Specific combination of physical parameters

Examples	Variables						Maximum of DSCF	DSIF
	ka	α_0	λ^{I}	λ^{II}	k^*	A^*		
A circular cavity in piezoelectric bi-material for case 6	0.1	0°	1	0.5	0.5	1.5	1.78	1.16
	1						5.24	0.20
	2						5.38	0.06
A circular cavity in piezoelectric bi-material for case 7	0.1	0°	1	0.5	0.5	1.5	1.78	1.16
		45°					1.24	–
		90°					2	–
A circular cavity in piezoelectric bi-material for case 8	2	0°	0.3	0.5	0.5	1.5	3.59	0.08
			0.5				3.91	0.08
			1				5.38	0.06
A circular cavity in piezoelectric bi-material for case 9	2	0°	1	0.3	0.5	1.5	6.91	–
				0.5			5.38	0.06
				1			4.36	–
A circular cavity in piezoelectric bi-material for case 10	2	0°	1	0.5	0.5	1.5	5.38	0.06
					1		4.85	–
					2		2.93	–
A circular cavity in piezoelectric bi-material for case 11	0.1	0°	1	0.5	0.5	1	1.78	0.16
						1.5	2.51	0.16
						2	3.13	0.15

7 Conclusion

In this paper, the Green's function method, mirror method, and crack-division method are applied to investigating the SH-wave scattering problem by a vertical interface crack and the nearby circular cavity in the piezoelectric bi-material half-space. Valuable numerical results under various combinations of parameters are obtained, which could provide references for practical engineering. The numerical analysis showed that the dynamic stress concentration factor (DSCF) around the circular cavity and dynamic stress intensity factor (DSIF) at the crack tip are affected by the incident wave, incident angle, the combination of medium parameters, and crack length to some extent. When the incident wave is at high frequency and vertical angle, the damage is serious. When medium II is softer than medium I, the damage is more serious. The longer the crack is, the more serious the damage would be. The influence of high frequency on the DSIF is obvious. A specific combination of physical parameters of the piezoelectric bi-material could decrease the DSCF, so a suitable combination of parameters can reduce the probability of structural fracture.

Acknowledgements The authors gratefully acknowledge the support from the Fundamental Research Funds for Central Universities (3072019CF0205).

References

1. Du, J.K., Pmydot, S.Y., Wang, X.: Scattering of anti-plane shear waves by a partially debonded piezoelectric circular cylindrical inclusion. Acta Mechanica **158**(3–4), 169–183 (2002). https://doi.org/10.1007/BF01176907
2. Shindo, Y., Moribayashi, H., Narita, F.: Scattering of antiplane shear waves by a circular piezoelectric inclusion embedded in a piezoelectric medium subjected to a steady-state electrical load. ZAMM Zeitschrift fur Angewandte Mathematik und Mechanik **82**(1), 43–49 (2002)
3. Song, T., Liu, D., Yu, X.: Scattering of SH-Wave and dynamic stress concentration in a piezoelectric medium with a circular hole. J. Harbin Eng. Univ. **23**(1), 120–123 (2002)
4. Song, T., Liu, D., Fu, G.: Dynamic anti-plane characteristic of piezoelectric medium with rigid cylindrical inclusion. J. Harbin Eng. Univ. **24**(5), 574–577 (2003)
5. Feng, W., Wang, L., Jiang, Z., Zhao, Y.: Shear wave scattering from a partially debonded piezoelectric cylindrical inclusion. Acta Mechanica Solida Sinica **17**(3), 258–269 (2004)
6. Shi, Y., Qi, H., Yang, Z.: Scattering of SH-wave by circular cavity in right-angle plane and seismic ground motion. Chin. J. Appl. Mech. **25**(3), 392–397 (2008)
7. Song, T.S., Li, D., Ren, Z.Y.: Dynamic anti-plane interaction between an impermeable crack and a circular cavity in an infinite piezoelectric medium. J. Mar. Sci. Appl. **7**(4), 297–301 (2008). https://doi.org/10.1007/s11804-008-7062-4
8. Yang, B.H., Gao, C.F., Noda, N.: Interactions between N circular cylindrical inclusions in a piezoelectric matrix. Acta Mechanica **197**(1–2), 31–42 (2008). https://doi.org/10.1007/s00707-007-0505-1
9. Song, T.S., Li, D.K.: Dynamic stress intensity factor for interfacial cracks of mode III on a circular cavity in piezoelectric bimaterials. Chin. J. Theor. Appl. Mech. **42**(2), 1219–1224 (2010)
10. Shu, X.: Analytical solutions of cross-ply piezoelectric composite laminates with various boundary conditions. Eng. Mech. **30**(4), 288–295 (2013)
11. Hassan, A., Song, T.: Smydot: Dynamic anti-plane analysis for two symmetrically interfacial cracks near circular cavity in piezoelectric bi-materials. Appl. Math. Mech. **35**(4), 1261–1270 (2014). https://doi.org/10.1007/s10483-014-1891-9
12. Wang, Y., Song, H., Gao, C., Xing, S.: The Anti-Plane Problem for a Cracked Elliptical Hole at the Interface of Bi-Materials. Chin. Q. Mech. **36**(3), 415–426 (2015)
13. Qi, H., Zhang, X.: Mmydot: scattering of SH-wave by a circular inclusion near the interfacial cracks in the piezoelectric bi-material half-space. J. Mech. **34**(3), 337–347 (2018). https://doi.org/10.1017/jmech.2017.7
14. Sahu, S.A., Kumari, S., Mondal, S., Pankaj, K.K.: Analysis of mechanical vibration (SH wave) in Piezo-composite plates. Mater. Res. Express **6**(6), 2019 (2019). https://doi.org/10.1088/2053-1591/ab5bd1
15. Li, D., Song, T.: Smydot: dynamic performance analysis of circular cavity near interface in piezoelectric bimaterials. Zhendong yu Chongji/Journal of Vibration and Shock **30**(3), 91–95 (2011)
16. Qi, H., Yang, J., Shi, Y.: Scattering of SH-wave by cylindrical inclusion near interface in bi-material half-space. J. Mech. **27**(1), 37–45 (2011). https://doi.org/10.1017/jmech.2011.5
17. Qi, H., Yang, J.: Dynamic analysis for circular inclusions of arbitrary positions near interfacial crack impacted by SH-wave in half-space. Eur. J. Mech. A Solids **36**, 18–24 (2012). https://doi.org/10.1016/j.euromechsol.2012.02.007
18. Lin, H., Liu, D.K.: Scattering of SH-wave around a circular cavity in half space. J. Earthq. Eng. Eng. Vib. **22**(2), 9–16 (2002)